Research Paper

EARTHQUAKE SPECTRA

Earthquake Spectra
1–27

DOI: 10.1177/87552930231170894
journals.sagepub.com/home/eqs
Sage

Evaluation of the optimal ground motion intensity measure in the prediction of the seismic vulnerability of earth dams

Gianluca Regina[1], Paolo Zimmaro, M.EERI[2,3], Katerina Ziotopoulou, M.EERI[4], and Roberto Cairo[1]

Abstract

The large majority of existing earth dams were designed with old standards, which often accounted for the effects of earthquakes in a simplified manner. As a result, seismic re-evaluation of these structures is now becoming increasingly important for dam owners. The seismic performance of earth dams can be evaluated at different levels of resolution, typically ranging from simple sliding block analysis, to the use of advanced numerical models. Seismic inputs for these models are typically chosen using code-based or site-specific probabilistic seismic hazard analysis (PSHA). In this study, we analyze the seismic vulnerability of two major earth dams located in Southern Italy, a seismically active area. The two dam systems have different geotechnical characteristics: one of them is founded on potentially liquefiable materials, whereas the other one is not susceptible to liquefaction. Our analyses are based on finite difference numerical simulations using both simplified and advanced constitutive models. Seismic vulnerability of both dams is analyzed by means of analytical fragility functions for various damage mechanisms and ground motion intensity measures (IMs). Such fragility functions are based on nonlinear deformation analyses within the multiple stripe analysis framework. We analyze efficiency and predictability of various IMs in predicting different damage levels and mechanisms. We show that the cumulative absolute velocity is overall the optimal IM in predicting vulnerability of both earth dams. We also analyze the relative importance of PSHA inputs (i.e. alternative ground motion and earthquake rupture forecast models; GMMs and ERFMs, respectively) and numerical models (simplified vs advanced) in the seismic analysis of earth dams by means of tornado diagrams. We show that the choice of GMMs and ERFMs

[1]Department of Civil Engineering, University of Calabria, Arcavacata di Rende, Italy
[2]Department of Environmental Engineering, University of Calabria, Arcavacata di Rende, Italy
[3]Department of Civil and Environmental Engineering, University of California, Los Angeles, Los Angeles, CA, USA
[4]Department of Civil and Environmental Engineering, University of California, Davis, Davis, CA, USA

Corresponding author:
Gianluca Regina, Department of Environmental Engineering, University of Calabria, Via P. Bucci, 87036, Arcavacata di Rende, Italy
Email: gianluca.regina@unical.it

is always more important than that of the constitutive model. However, for dams prone to liquefaction, the choice of the constitutive model has a higher importance than for non-liquefiable earth dams.

Keywords
Earth dams, fragility functions, efficiency, vulnerability, tornado diagrams

Date received: 27 July 2022; accepted: 22 March 2023

Introduction

Earth dams are critical infrastructure systems that can serve various functions and are particularly important for the resilience of entire communities following major natural and/or anthropogenic disasters. Most existing embankment dams worldwide were built after the Second World War (Penman, 1986). This means that they were designed with older codes and often without considering seismic actions. For this reason, many countries, including Italy and the United States, launched nation-wide initiatives to perform seismic re-evaluations of existing dams (e.g. the USA National Dam Safety Program of 1996 and subsequent modifications, and the Italy National seismic re-evaluation of large dams of 2003–2004). Such seismic re-evaluations need to be performed using site-specific and hazard-consistent ground motions and, ideally, robust probabilistic metrics to identify dam's vulnerability. The seismic probabilistic assessment of strategic infrastructure systems is typically performed following a two-step approach. First, the seismic hazard is estimated by means of a probabilistic seismic hazard analysis (PSHA). Then, the seismic performance is addressed using fragility functions which, for any given level of a ground motion intensity measure (IM), provide the probability that the structure reaches (or exceeds) a certain limit state (or damage measure, DM). Mathematically, they represent the following conditional probability:

$$P(d > \mathrm{DM} | \mathrm{IM} = x) \tag{1}$$

There are three general approaches to build a fragility function: (1) analytically (i.e. based on the results of numerical models), (2) empirically (i.e. based on empirical data), and (3) based on expert judgment. In this study, analytical fragility functions are considered. Details about the other methodologies can be found in Porter (2017). Fragility functions can also be defined as the cumulative distribution function (CDF) of the resistance to a certain damage state of the analyzed structure. A lognormal CDF is typically used to represent the above probability:

$$P(d > \mathrm{DM} | \mathrm{IM} = x) = \Phi\left(\frac{\ln \frac{x}{\theta}}{\beta}\right) \tag{2}$$

where ϕ is the standard normal CDF, x is the IM, θ is the IM that corresponds to 50% probability of exceedance (i.e. the median value), and β is the standard deviation of the natural logarithm of the IM (also called dispersion). The real values of θ and β are unknown, so they must be estimated using statistical procedures. For instance, in a cloud analysis, the β is evaluated as the standard deviation of a logarithmic linear regression between the IM and DM, and θ as the median value of the IM distribution (Di Sarno and Elnashai, 2021). More information about typical methods available to compute fragility

functions for structural and infrastructural systems are provided by Baker (2015). In this study, the multiple stripe analysis (MSA) procedure is adopted, which is based on the maximum likelihood method. Thus, the θ and β are estimated through a fitting procedure. Fragility functions for a given structure or structural type can be used to various scopes, including (1) rapid post-earthquake assessments of the damage produced to a large structure or infrastructure portfolio (e.g. city-scale structural damage assessments or rapid damage assessments by dam owners) and (2) infrastructure early warning systems triggered if a given damage level is expected to be exceeded (e.g. Pagano and Sica, 2012). However, it is not practical to perform probabilistic seismic demand models for several IMs, as the computational effort of the numerical analyses would be large. Hence, the choice of the IM to use in such applications is very important. Typically, the IM to be used is that which correlates well with a certain DM. The issue of determining the optimal IM to use in forward analyses is important for various reasons. Deterministic seismic hazard analyses are still widely used in dam engineering (Wong and Thomas, 2017). Thus, a target IM must be chosen to perform such analyses. For deterministic studies, it is of paramount importance that the selected IM correlates well with a DM (often-called Engineering Demand Parameter, EDP) because it is the only parameter that defines the seismic hazard level. If the IM and DM are poorly correlated, a small variation in the IM level (and thus a small variation of the seismic hazard level) could lead to a large variation in the expected DM. IM-DM relationships are also crucial for coupled analyses of earth dams, which comprise the hazard estimation and seismic response evaluation procedures with probabilistic approaches (i.e. site-specific PSHA and fragility functions). The correlation between an IM and the target DM can be synthesized by a single property of the selected IM: its efficiency (i.e. how well the IM is correlated with a given DM).

Ideally, the optimal IM to be selected has to be sufficient too (Luco and Cornell, 2001). Sufficiency measures the dependence of the DM, for a given IM, on the magnitude (M) and source-to-site distance (R) of the ground motion. If the IM is sufficient, the information on M and R does not reduce the variability of the DM. In such a case, the efficiency of a ground motion IM is solely evaluated by the standard deviation of the DM for a given IM. In particular, the natural logarithm of the IM and DM is first calculated, and then a least-square linear regression is performed. The root mean square error of the regression is the logarithmic standard deviation $\sigma_{\ln DM|\ln IM}$ and represents the efficiency of the IM. The sufficiency of the selected ground motion IMs was not explored in this article. However, some insights into this issue are provided by Yang (2021) for levees.

The third property of an optimal IM is predictability. This property is important in forward applications, because if an efficient IM cannot be reliably estimated, the whole methodology would produce an unexpectedly high level of uncertainty. As a result, in addition to being efficient and sufficient, an optimal IM should also be predictable. Predictability can be easily identified as the standard deviation produced by the prediction model used to estimate a given IM. The optimal IM varies depending on the structure and on the DM considered (Karimi and Dashti, 2017; Nguyen et al., 2021). For earth dams, however, a small number of studies analyze the relationship between IM-DM and how it relates to fragility functions (e.g. Armstrong et al., 2021).

In this study, a probabilistic seismic demand analysis is performed for two earth dams in Southern Italy: the Farneto del Principe and the Angitola dams, both located in the Calabria region. MSA-based fragility functions are derived for several IMs and DMs. Using these results, we then identify optimal IMs for both earth dam types (susceptible and non-susceptible to liquefaction), by calculating the total standard deviation of each

Table 1. Summary of the standard deviation of the fragility functions for earth structures.

Study	Dam type	Method	Damage measure	Intensity measure	β[a]
Hurtado-López and Mayoral-Villa (2020)	Concrete-face Hardfill	Analytical (IDA)	Shear stress/ strength	PGA	0.569–0.614–0.572
Figura (2020)	Small earth dam	Analytical	Crest settlement	PGA	1.093
				PGV	1.078
			Horizontal displacement	PGA	1.208
Kwak et al. (2016)	Levee	Empirical	Damage-level index based on crest settlement, crack depth, and crack width	PGV	0.92
				PGA	1.07
Jin and Chi (2019)	Earth-rockfill dam	Analytical (MSA)	Damage based on relative settlement ratio	PGA	0.33
Bernier et al. (2016)	Concrete gravity dam	Analytical (MSA)	Sliding	$Sa(T_{fund})$	0.36–0.57
SYNER-G Reference Report 4 (Kaynia, 2013)	Roadway embankments	Analytical	Damage state based on permanent ground displacement	PGA	1–0.9–0.7
Tsai (2018)	Levee	Empirical (MLE)	Damage level based on crack dimensions and subsidence	PGA	0.56-0.88

PGA: peak ground acceleration; PGV: peak ground velocity; MSA: multiple stripe analysis; IDA: Incremental Dynamic Analysis; MLE: Maximum Likelihood Estimation.

[a]Ranges are reported for fragility functions referring to the same infrastructure, but different intensity measures and or damage measures.

considered IM that includes both efficiency and predictability. Results are then compared against a recent study on two earth dams in California (Armstrong et al., 2021): the Lenihan and Anderson dams. The latter is susceptible to liquefaction, while the former is not (Dorsey, 2011; Kuhl, 2011). In addition to focusing on different earth dams located in different regions, this study is different from that of Armstrong et al. (2021) as they did not perform MSA but a more traditional type of nonlinear deformation analyses (NDAs) with unscaled ground motions, chosen to be consistent with the seismic hazard of several dams in California. Presently, the number of seismic analytical fragility functions for earth dams is very limited and always based on input selections performed using uniform hazard spectra (UHS) (e.g. Jin and Chi, 2019; Vecchietti et al., 2019, both for rockfill dams). Table 1 summarizes the main studies on fragility functions on some infrastructure systems, for different DM and IM; the dispersion β is also reported. It should be noted that these studies adopt different methodologies and that a direct comparison between the dispersion β is not truly meaningful. However, it provides an idea on the overall range of values that can be expected when performing these types of analyses.

In addition to producing MSA-based fragility functions for two earth dams in Southern Italy and providing useful insights on the optimal IM to be used when analyzing potentially liquefiable and non-liquefiable earth dams, we also evaluate the relative importance of PSHA input parameters and the level of sophistication of constitutive models in the

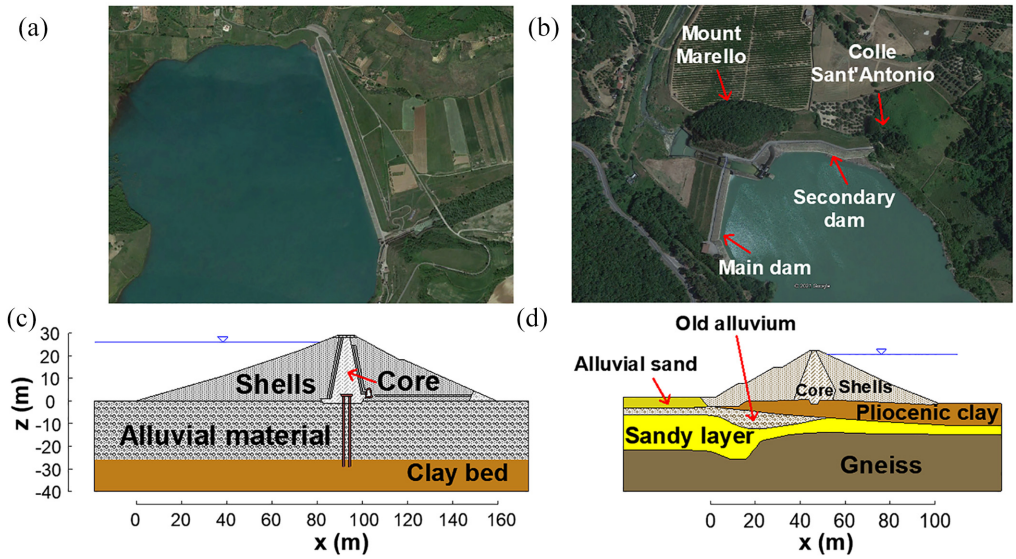

Figure 1. (a, b) aerial views and (c, d) cross sections of the Farneto del Principe and Angitola dams, respectively.

seismic analysis of earth dams. This assessment is performed using an approach reliant upon tornado diagram analyses based on alternative ground motion and earthquake rupture forecast models (GMMs and ERFMs, respectively) and constitutive models (simplified vs advanced). Such analysis is particularly relevant for earth dams' owners and managers as it can guide fund allocation and prioritization processes more efficiently using a repeatable, quantitative, and technically defensible approach.

Case studies

The Farneto del Principe dam

The Farneto del Principe dam (Figure 1a) is a zoned earth dam located in the Calabria region (Southern Italy, latitude 39.6515°N, longitude 16.1627°E), a seismically active region characterized by the presence of shallow crustal faults and deep seismicity related to the subduction zone of the Calabrian Arc. The dam height is 30 m and its length is more than 1200 m. The geotechnical characterization of the Farneto del Principe dam is based on a comprehensive field investigation program (Regina et al., 2021), showing that both, the dam and the foundations, are not susceptible to liquefaction. The water tightness of the dam system is ensured by a central core made of compacted, low permeability clay and silt. Its static stability is ensured by the shells, which comprise sand and gravel. Two filters (with thickness of 1 m each) protect the dam core, with grain size distributions similar to that of the adjacent soil, both upstream and downstream. The foundation of the dam comprises a shallower layer of high-permeability alluvial material (i.e. sand and gravel) which is in turn founded on a thick clay layer. The exact location of the compliant bedrock is unknown. A cut-off wall is present throughout the length of the dam within the alluvial material and embedded for 3 m into the clay bed, to prevent groundwater flow and possible underseepage. Downstream of the core an inspection tunnel is present. Figure 1c shows a representative cross section of the dam.

The Angitola dam

The Angitola dam (Figure 1b; latitude 38.7486°N and longitude 16.2319°E) is a zoned earth dam located in the same tectonic context of the Farneto del Principe dam (the two dams are 130 km apart). The structure comprises two dams located on the two sides of Mount Marello. One of these dams is founded on soils that are potentially susceptible to liquefaction and thus it was selected to be the objective of this study. This decision was made to compare fragility results between a dam without liquefaction issues and another one with potential liquefaction-prone soils. The dam height is 27.75 m and its length is about 195 m. The core of the dam comprises medium plasticity silty sands, while the shells are composed of sandy gravel. There are two filters separating the core and the shells; the internal filter, adjacent to the core, is 60 cm thick and comprises sand and gravel, while the external filter is 140 cm thick. The foundation layers are characterized by a complex geology. On the downstream side, there is a 5-m-thick layer of sandy silts, which comprises recent alluvial material that is susceptible to liquefaction. Beneath this layer, there is an old alluvial material comprising gravel with sandy silt, together with tiny fractions of clay material. The dam lays on a pliocenic formation of consistent silty clay, whose thickness rises longitudinally from the downstream to the upstream side. Beneath those layers, a heterogeneous sand layer (with soil particles comprising gravel, sand, silt, and clay) is present, coming from the weathering of the underlying rock foundation (sandy layer), which is made up of fractured gneiss. The intact rock is about 40 m below the free surface. A representative cross section of the dam is shown in Figure 1d.

Methodology

Numerical modeling

The numerical modeling of the two case studies is performed with the 2D finite difference commercial software platform FLAC (Itasca, 2019) which is based on the explicit, time-marching method to solve the equations of motion. The mesh was designed to ensure an accurate wave propagation process (Lysmer and Kuhlemeyer, 1973) and to capture geometric details (such as the filter). At the edges of the models, the mesh has a maximum width of 2 m, while in the center of the model the mesh elements are squared with a size equal to 0.6 m $\times$ 0.6 m. Figure 2 shows the meshes of the two analyzed dams. At the base of the model, quiet boundaries are used to simulate the elastic half-space. On the lateral boundaries of the model, the free-field boundary condition is adopted to ensure radiation damping toward infinity. The initial stress state is estimated for both dams with a six-stage process, based on data from the construction logs of the dams. Seepage analyses are performed with an uncoupled fluid-flow calculation. The results of such analyses were calibrated following a comparison against available piezometer data (Ausilio et al., 2016). Three different constitutive models are used in this study. For the materials susceptible to liquefaction (only present in the Angitola dam), the PM4Sand V3.1 model is adopted (Boulanger and Ziotopoulou, 2017). The behavior of the foundation bedrock is assumed to be linear elastic, while all the other materials are characterized by the Mohr-Coulomb (MC) failure criterion coupled with a simplified hysteretic procedure (Itasca, 2019). PM4Sand is a plane strain–stress ratio–controlled, critical state–compatible, bounding surface plasticity model. The calibration of this model is performed with single-element simulations for the range of loading paths important for the dam. In this study, the PM4Sand parameters are calibrated to obtain a cyclic resistance curve to liquefaction that matches that estimated from empirical procedures (Boulanger and Idriss, 2014). More details about

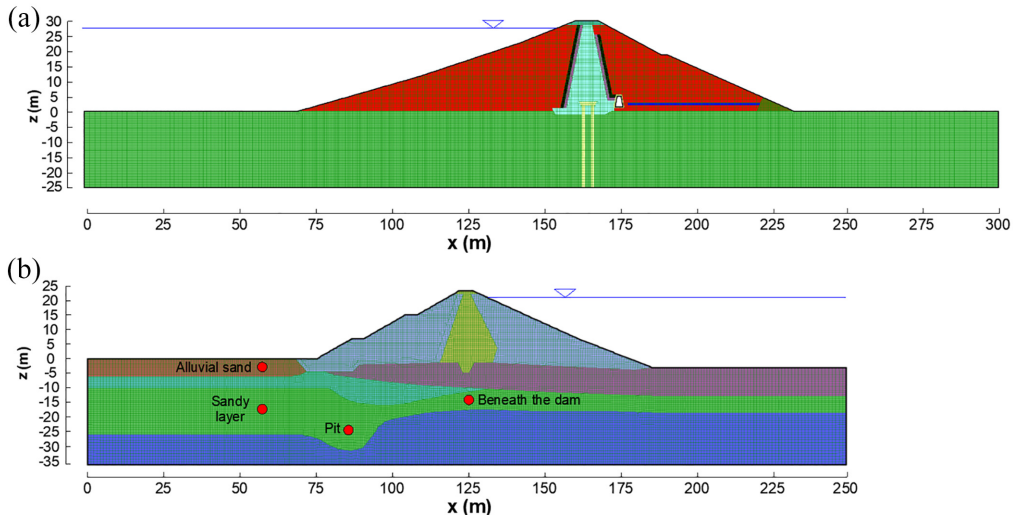

Figure 2. Meshes of the analyzed dams: (a) Farneto del Principe dam and (b) Angitola dam (red dots in this figure represent control points for liquefaction-related analysis).

Table 2. Parameters adopted for the Farneto del Principe dam.

Property	Core	Shells	Alluvium
γ (kN/m^3)	20.2	24.1	24.1
c' (kPa)	16.5	0	0
ϕ' (°)	22.4	40	37.5
G (MPa)	$G(z)$	$G(z)$	$G(z)$

the calibration of the PM4Sand model and the numerical modeling are provided by Regina (2021). Modeling parameters for both dams and constitutive models are presented in Tables 2 and 3. We adopted a variation of the shear modulus with depth (i.e. or mean effective stress), based on available field investigation data (Regina, 2021). For both dams, a 0.5% Rayleigh damping with a central frequency of 3 Hz is used to remove high frequency noise. The inspection tunnel of the Farneto del Principe dam (Figure 1a) was explicitly modeled as an elastic material with a Young's modulus of 30,500 MPa and a Poisson ratio equal to 0.2.

Multiple stripe analysis procedure

The MSA procedure is often used to define fragility functions of structures and/or infrastructure systems using outcomes of numerical simulations. In this procedure, numerical analyses of the seismic performance of a given structure are performed at discrete IM levels, typically corresponding to given return periods of the seismic action (i.e. each IM level represents a stripe). For each IM level, various ground motions are used in the analysis. The MSA method works well especially when ground motions are selected and scaled to be consistent with a conditional spectrum. This is because the ground motion target properties change at each IM level and thus the representative ground motions do so as well (Lin et al., 2013). In the MSA, the results of the numerical simulations are used to identify

Table 3. Parameters adopted for the Angitola dam.

Property	Core	Shells	Pliocenic clay	Old alluvium	Sandy layer			Alluvial sand	Gneiss
γ (kN/m^3)	20.36	21.92	18.25	18.5	18.5			19.5	25.5
c' (kPa)	10	0	48	0	0			0	-
ϕ' (°)	26	40	24	35	34.5			36	-
G (MPa)	$G(z)$	$G(p')$	$G(p')$	$G(p')$	$G(p')$			$G(p')$	1880
D_R (%)	–	–	–	–	67.0	58.4	58.4	39	–
G_0	–	–	–	–	810	2250	3400	800	
h_{p0}	–	–	–	–	3.0	0.25	1.0	5.5	–

The three different values of the PM4Sand parameters (D_R, G_0, and h_{p0}) refer to different zones of the model (free field condition, pit zone, and beneath the dam).

the number of ground motions that cause an exceedance of the DM of interest. Under the assumption that the exceedance of one DM is independent of the GM, the probability of having z_j exceedances in n_j GMs with IM = x_j is given by the following binomial distribution:

$$\text{Fraction of exceedances} = \binom{n_j}{z_j} p_j^{z_j} \left(1 - p_j\right)^{n_j - z_j} \tag{3}$$

The index j spaces on the number of IMs chosen to perform the MSA (i.e. the number of stripes). The fraction of exceedances are known from the analyses, and p_j is the probability of observing an exceedance with IM = x_j, which is the unknown fragility function. A lognormal CDF is used for the p_j, and the maximum likelihood method is exploited to estimate parameters θ and β, providing the CDF that gives the highest probability of observing the exceedances computed from the analyses. When multiple IM levels are used, the likelihood is computed as the product of the binomial distributions. Finally, maximizing this function for θ and β, the fragility function is obtained:

$$\text{Likelihood} = \prod_{j=1}^{m} \binom{n_j}{z_j} \Phi\left(\frac{\ln \frac{x}{\theta}}{\beta}\right)^{z_j} \left[1 - \Phi\left(\frac{\ln \frac{x}{\theta}}{\beta}\right)\right]^{n_j - z_j} \tag{4}$$

MSA-based fragility functions for different IMs

This section presents fragility functions for both dams analyzed in this study, calculated using results from the MSA procedure, for several damage classes and intensity measures. The objectives of this section are to (1) present fragility functions for the case studies that can be used in the future for early warning systems and/or rapid post-earthquake assessments, and (2) identify appropriate IMs that relate well with the predicted limit state and DM. Such appropriate IMs would be those producing low dispersions (i.e. lower values of β). It should be noted that the fragility functions presented here are specific to the two case studies presented in this article. However, they can be used to make rapid assessments (perhaps when large dam portfolios are analyzed) on dams with similar characteristics. The choice of the input ground motions to be used in the analysis is conducted using a conditional spectrum as target (Baker, 2011) and the fundamental period of the dam as the conditioning period. These types of response spectra are also called scenario target

spectra, which are consistent with a scenario characterized by a certain magnitude, distance, and rate of occurrence. The controlling scenarios for the sites of interest are identified with the disaggregation of the seismic hazard, for six different return periods, T_R (75, 475, 710, 1460, 1950, and 2475). Supplemental Figures S21–S24 show PSHA results for both dam sites and all considered T_R. For each T_R, 7 to 10 inputs were selected to capture the uncertainties related to ground motion variability. This relatively high number of ground motions per IM level ensures that the ground motion uncertainties are captured (Figura, 2020; Hurtado-López and Mayoral-Villa, 2020). More details about the ground motion selection, scaling process, and estimation of the fundamental period of the dam are provided by Regina (2021). Five IMs are used to construct analytical fragility functions for the case studies: (1) peak ground acceleration (PGA), (2) peak ground velocity (PGV), (3) Arias intensity (AI), (4) cumulative absolute velocity (CAV), and (5) cumulative absolute velocity above 5 cm/s^2, CAV5 (Kramer and Mitchell, 2006). CAV and CAV5 were selected as previous studies (e.g. Armstrong et al., 2021; Bray and Macedo, 2017; Karimi and Dashti, 2017; Kramer and Mitchell, 2006) showed their ability in predicting liquefaction-related damage. An additional DM is also considered for the Angitola dam: the excess pore water pressure ratio r_u at the end of shaking:

$$r_u = \frac{\Delta u}{\sigma'_c} \tag{5}$$

where Δu is the excess pore water pressure that develops in the soil during shaking and σ'_c is the effective consolidation stress before shaking. Time series of r_u are calculated in four different zones of the model when performing the analyses with the PM4Sand constitutive model (red dots in Figure 2): (1) in the alluvial sand; (2) in the sandy layer, downstream; (3) in the pit zone of the sandy layer, where the static pre-earthquake pore pressure is high; and (4) in the sandy layer beneath the dam. Four thresholds of r_u are adopted to define the fragility functions, to track the evolution of excess pore pressure at these control points. High values of r_u (i.e. when it is approaching 100%) are representative of liquefaction initiation. Lower values of r_u are useful to appreciate shear strength reduction during shaking as a result of excess pore pressure generation mechanisms. For PGA, selected ground motions used in the analysis are scaled at the amplitude level derived from the M-R-ε disaggregation results (i.e. the PGA that is most likely to be expected at the corresponding M-R-ε scenario). A summary of the PGA disaggregation results for both dam sites is reported in the electronic supplement to this article. The GMMs used in the site-specific PSHA for this study do not allow for the estimation of AI, CAV, and CAV5. Hence, it was not possible to compute their mean values from disaggregation results and to scale the GMs to those values. Because of this reason, and to reduce the number of site-specific PSHA and disaggregation analyses to be performed, PGA-based GMs were used for all other IMs. In other words, to build non-PGA-based fragility functions (i.e. those using IMs different from PGA), we used the same GMs used to generate PGA-based fragility curves (for which median PGA values are known at each return period). When applied to IMs different from PGA, this approach generated stripes (i.e. suites of GMs at the same T_R) with variable IM values. However, since each stripe should have corresponding GMs with constant IM values, we rescaled each GM with different scaling factors for each non-PGA IM. In this procedure, we first organized IM values for each T_R and defined, for non-PGA IMs, the median IM value corresponding to that T_R. Then, we calculated the applicable scaling factor to achieve, for any given T_R, the target median IM value. All ground motions used for the analyses and their main characteristics, including scaling factors, are reported in the electronic supplement.

Table 4. Pells and Fell (2003) damage classes for the Farneto del Principe and Angitola dams.

Damage class		Farneto del Principe		Angitola	
No.	Description	Maximum longitudinal crack width (mm)	Maximum relative crest settlement (cm)	Maximum longitudinal crack width (mm)	Maximum relative crest settlement (cm)
0	None or slight	<10	$\leqslant 1$	<10	$\leqslant 0.8$
1	Minor	$10 < w \leqslant 30$	$1 < d \leqslant 6$	$10 < w \leqslant 30$	$0.8 < d \leqslant 5.4$
2	Moderate	$30 < w \leqslant 80$	$6 < d \leqslant 15$	$30 < w \leqslant 80$	$5.4 < d \leqslant 13.5$
3	Major	$80 < w \leqslant 150$	$15 < d \leqslant 45$	$80 < w \leqslant 150$	$13.5 < d \leqslant 40.5$
4	Severe	$150 < w \leqslant 500$	$45 < d \leqslant 150$	$150 < w \leqslant 500$	$40.5 < d \leqslant 135$
5	Collapse	>500	>150	>500	>135

Various DMs can be identified for earth dams. The following DMs were considered to perform MSA and construct fragility functions in this study:

1. *Filters displacement*. Following Seed (1979) protocols, the limiting filter displacement value is defined as one time the filter thickness, t_f. For the Farneto del Principe dam, this limiting value is equal to 1 m, while for the Angitola dam, t_f is equal to 1.4 m. In the numerical model, such values are taken as displacement vector amplitudes. Additional values of the limiting displacement for this damage mechanism were also considered (i.e. 0.5 and 0.25 m for the Farneto del Principe dam and 0.7, 0.6, and 0.3 m for the Angitola dam).
2. *Global instability*. This damage mechanism refers to permanent displacements occurring within the dam body and in the dam's foundation. In the numerical model, this displacement value is taken as the total displacement within the failure surface defined by the zone where the maximum shear strains are concentrated. The maximum allowable displacement for this mechanism is taken as 1 m. Additional values of the limiting displacement for this damage mechanism were also considered (i.e. 0.50, 0.25, and 0.15 m).
3. *Free board reduction*. This damage measure corresponds to the settlement of the upstream vertex of the crest. If it is greater than the free board, the collapse limit state is reached. Damage measures corresponding to 65%, 50%, and 25% of the maximum free board settlement that would lead to collapse are also considered.
4. *Pells and Fell damage classes*. This damage measure is based on the empirical results obtained by Pells and Fell (2003). It has been recently used by Rathje and He (2022) within a framework to define seismic probabilistic fragility for earth dams. Their empirical methodology defines five damage classes (DCs), which are related to the vertical displacement of the crest. Table 4 reports all DCs considered in the analysis of the Farneto del Principe and Angitola dams.
5. *Normalized Crest Settlement* (NCS). This damage measure is based on the Swaisgood (2003, 2014) empirical methodology. The author analyzed the damage to several earth dams observed after strong earthquakes and related it to NCS, which is defined as follows:

$$\mathrm{NCS} = \frac{\Delta}{H+s}100\% \tag{6}$$

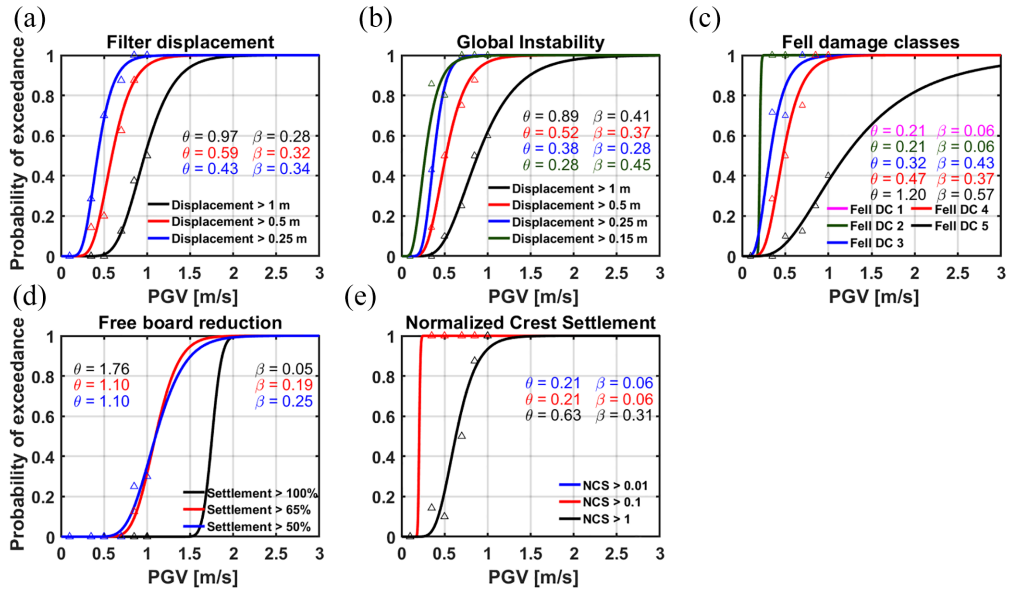

Figure 3. Fragility functions for the Farneto del Principe dam conditioned on PGV: (a) Filter displacement; (b) Global instability; (c) Fell damage classes; (d) Free board reduction; (e) Normalized Crest Settlement.

where Δ is the mean vertical settlement of the crest, H is the dam height, and s is the foundation thickness. It should be noted that in the study by Swaisgood (2014), all dams that reported a value of NCS greater than one are those where liquefaction occurred. Such conditions (liquefiable dam and/or dam's foundation material) are not met by the Farneto del Principe dam. As a result, this DM is not necessarily accurate to describe high displacements for this dam. We recognize that some of these DMs are correlated between each other. However, we decided to use them all as they are the most used DMs in the literature. As a result, it is valuable providing fragility functions (and related observations) for all of these DMs.

In the subsequent subsections, analytical fragility functions for both dams are presented for various IMs, DMs, and constitutive models. All fragility functions shown in the text are conditioned on PGV as it has been shown a good IM for dam and levee applications (e.g. Armstrong et al., 2021; Kwak et al., 2016). Additional fragility functions for other IMs are provided in the Electronic Supplement to this article. Summary tables for all IMs are provided in the remainder of this section.

Analytical fragility functions for the Farneto del Principe dam

Figure 3 shows analytical fragility functions conditioned on PGV for the Farneto del Principe dam. The model fitting to the data is relatively good and there is a consistent trend of the fraction of GMs that exceeds a certain threshold (i.e. open triangles) with increasing values of the IM. The standard deviation β is an indicator of the goodness of fit. For PGV, the β are relatively low for all analyzed DMs (ranging between 0.10 and 0.60). Figure 4 shows the DM that is most likely to be exceeded for a certain value of the IM at the collapse limit state. This figure shows that some damage states are more likely to be exceeded than others for the same level of PGV. Such differences should be carefully

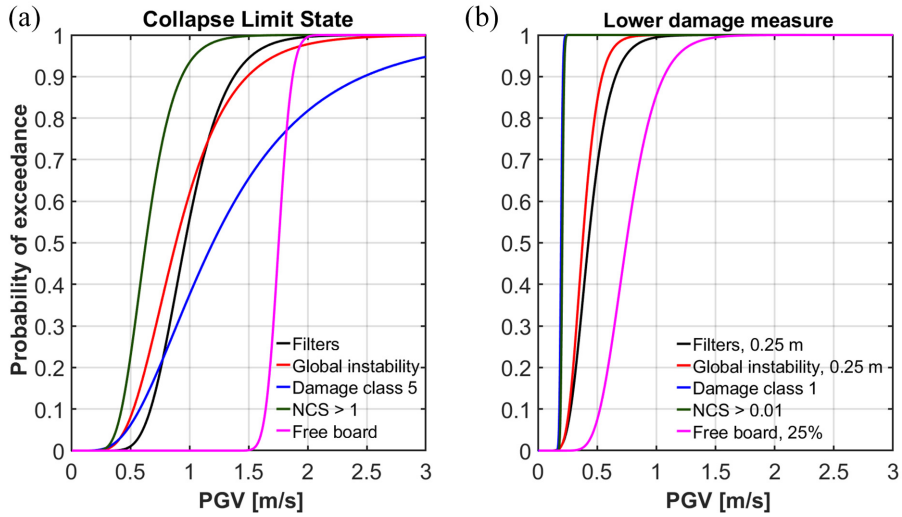

Figure 4. Comparison between fragility functions for two selected limit states: (a) collapse limit state and (b) lower damage measures.

accounted for when using fragility functions for forward analyses. The filters and global instability DMs have similar probabilities of exceedance given a certain level of PGV (i.e. fragility functions are close to each other). These fragility functions are much different than the free board reduction functions (which have a high standard deviation). This is somewhat expected, as the freeboard of the Farneto del Principe dam is 2.5 m, a displacement threshold significantly higher than the 1 m limit for filters and global instability.

Fragility functions can also give information on how much damage the dam can still sustain before reaching collapse. The difference between the probability of exceeding a serviceability damage state and a collapse state for a certain value of IM is shown in Figure 4. Figure 4b shows the probabilities of exceedance of lower damage measures (i.e. fragility functions are defined with lower damage thresholds). For these fragility functions, the return period of each ground motion stripe is unknown. Figure 4b shows that it is more likely to get a permanent displacement of 25 cm in the shells than the same displacement value in the filters. This is consistent with the shear strain and displacement spatial patterns observed and shown in Figure 5 (which shows shear strain values at the end of one representative earthquake that was selected among those used to derive fragility functions for this dam), which suggest collapse mechanisms concentrated near the abutments.

Table 5 reports the IMs used in the MSA for the Farneto del Principe and Angitola dams. Table 6 shows median and standard deviation values of all fragility functions obtained for the collapse limit state for different IMs for the Farneto del Principe dam. CAV and CAV5 generally produce the lowest values of β for all DMs. AI consistently has the highest values of β across all DMs. PGA generally has higher β values than CAV, CAV5, and PGV, and lower values of β than AI.

Analytical fragility functions for the Angitola dam

In this section, analytical fragility functions for the Angitola dam are presented. Figure 6 shows the results obtained for the MC dam model (i.e. this is not a model purely based on

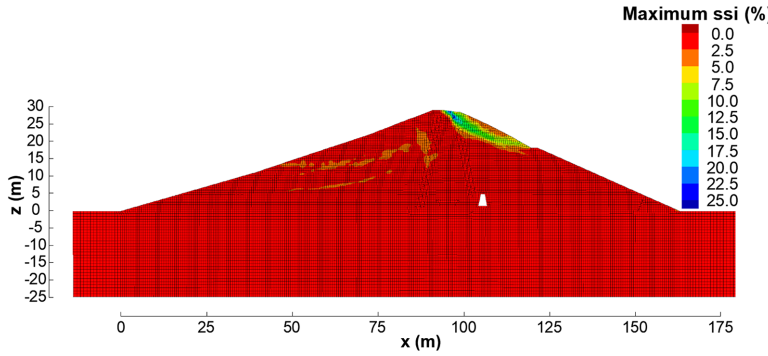

Figure 5. Maximum shear strain increment (ssi) values at the end of one earthquake for a representative analysis of the Farneto del Principe dam.

Table 5. IMs adopted for the MSA of the Farneto del Principe and Angitola dams.

Farneto del Principe dam					
Return period	PGA [g]	PGV [m/s]	AI [m/s]	CAV [m/s]	CAV5 [m/s]
75	0.206	0.1	1	6	5
475	0.512	0.35	5	12	11
710	0.617	0.5	10	15	15
1460	0.797	0.7	15	25	26
1950	0.884	0.85	20	30	31
2475	0.962	1	25	35	34
Angitola dam					
Return period	PGA [g]	PGV [m/s]	AI [m/s]	CAV [m/s]	CAV5 [m/s]
75	0.208	0.075	0.5	4	2
475	0.531	0.15	2	7.5	6
710	0.626	0.25	3	10	9
1460	0.820	0.4	4.25	13	12

IM: intensity measure; MSA: multiple stripe analysis; PGA: peak ground acceleration; PGV: peak ground velocity; AI: Arias intensity; CAV: cumulative absolute velocity; CAV5: cumulative absolute velocity above 5 cm/s2.

Table 6. Median and standard deviations of the Farneto del Principe dam fragility functions for the collapse limit state.

Ultimate limit state condition										
IM	Filters		Global instability		Free board reduction		Fell damage class 5		Normalized crest settlement	
	θ	β	θ	β	θ	β	θ	β	θ	β
PGA [g]	1.24	0.38	1.28	0.38	2.67	0.57	1.35	0.46	0.94	0.31
PGV [m/s]	0.97	0.28	0.89	0.41	1.76	0.05	1.20	0.57	0.63	0.31
AI [m/s]	26.33	0.68	22.97	0.64	n.a.	n.a.	31.96	0.67	8.93	0.48
CAV [m/s]	35.39	0.02	35.18	0.02	n.a	n.a	n.a.	n.a.	26.92	0.28
CAV5 [m/s]	45.27	0.26	37.45	0.39	n.a.	n.a.	n.a.	n.a	23.78	0.24

N.a. means that no settlements greater than the free board were observed. IM: intensity measure; PGA: peak ground acceleration; PGV: peak ground velocity; AI: Arias intensity; CAV: cumulative absolute velocity; CAV5: cumulative absolute velocity above 5 cm/s^2.

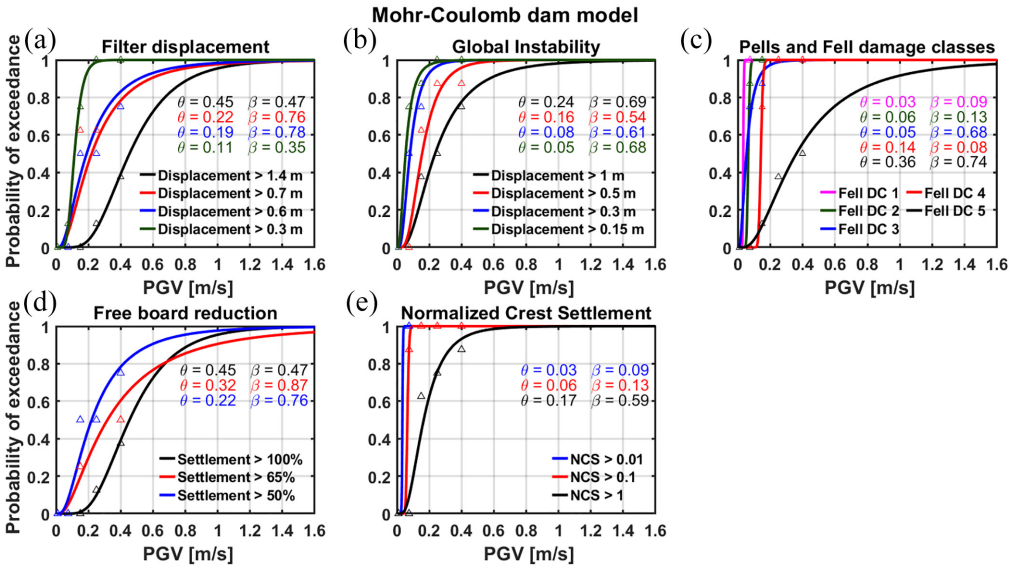

Figure 6. Fragility functions for the Angitola dam conditioned on PGV (Mohr-Coulomb dam model): (a) Filter displacement; (b) Global instability; (c) Fell damage classes; (d) Free board reduction; (e) Normalized Crest Settlement.

the MC criterion, but rather, a MC model coupled with a simplified hysteretic procedure, Itasca, 2019); this model was used for all materials of the dam and its foundation—in the remainder of the article, we will refer to this model as the "MC dam model" or simply "MC model" for several DMs. There are consistent trends between fragility functions for different DMs, with most of them similar to those observed for the Farneto del Principe dam. Overall, there are increasing fractions of exceeding DMs with increasing IM values. However, some apparent numerical inconsistencies are present. For instance, for the free board reduction fragility function conditioned on PGV, the settlement greater than 100% curve (i.e. black curve in Figure 6) overlaps with the red curve at around 80% (i.e. settlement $> 65\%$). This seems counterintuitive at first. However, such an effect may be the result of variability (i.e. the set of ground motions used at the return periods adopted in these analyses are not the same for the two fragility functions). Hence, a more intense GM can produce smaller damage than a lower-intensity GM, if the latter has some specific characteristics (such as long duration, a frequency content close to the fundamental frequency of the dam, and/or a particularly high energy content).

The CAV and CAV5 fragility functions are quite similar, as expected. For these two IMs, the GM scaling factors were very similar. Table 7 shows θ and β values for all IMs using the MC model. The AI produces fragility functions with the highest β values. This observation is consistent with what was observed for the Farneto del Principe dam. Similarly, CAV and CAV5 are the IMs producing the lowest values of β. The only exception to this trend is the fragility curve for the Normalized Crest Settlement, where the PGV-based fragility curve has a slightly lower β value than CAV5 (and similar to that obtained with CAV). Interestingly, this is the only DM for which the lowest value of β is obtained for the PGV-based fragility curve. Figure 7 shows PGV-based fragility functions for the Angitola dam using the PM4Sand model for potentially liquefiable materials. This advanced constitutive model is used to capture excess pore pressure build-up and

Table 7. Comparison between median and standard deviation values of the fragility functions of the Angitola dam for the MC and PM4Sand models, for all considered collapse limit states.

Collapse limit state, MC dam model										
IM	Filters		Global instability		Free board reduction		Fell damage class 5		Normalized crest settlement	
	θ	β	θ	β	θ	β	θ	β	θ	β
PGA [g]	0.81	0.20	0.46	0.40	0.94	0.52	0.65	0.50	0.26	0.80
AI [m/s]	4.62	0.44	1.25	0.86	4.69	0.35	2.29	0.49	0.51	1.52
PGV [m/s]	0.46	0.47	0.24	0.69	0.45	0.47	0.36	0.74	0.17	0.59
CAV [m/s]	12.87	0.03	8.85	0.28	13.14	0.03	10.69	0.16	4.75	0.61
CAV5 [m/s]	11.54	0.03	7.48	0.36	11.86	0.04	9.26	0.20	3.62	0.83
Collapse limit state, PM4Sand dam model										
IM	Filters		Global instability		Free board reduction		Fell damage class 5		Normalized crest settlement	
	θ	β	θ	β	θ	β	θ	β	θ	β
PGA [g]	0.88	0.24	0.44	0.70	0.88	0.24	0.88	0.67	0.26	0.80
AI [m/s]	4.69	0.35	1.50	0.95	4.31	0.05	3.44	0.27	0.38	1.70
PGV [m/s]	0.45	0.47	0.30	1.00	0.45	0.47	0.38	0.47	0.18	0.63
CAV [m/s]	13.33	0.04	8.00	0.35	n.a.	n.a.	11.45	0.18	4.11	1.05
CAV5 [m/s]	12.00	0.03	7.84	0.38	12.64	0.04	10.02	0.23	3.41	0.72

N.a. means that no exceedances were observed. IM: intensity measure; PGA: peak ground acceleration; AI: Arias intensity; PGV: peak ground velocity; CAV: cumulative absolute velocity; CAV5: cumulative absolute velocity above 5 cm/s^2.

dissipation during the seismic excitation. Table 7 summarizes θ and β values of the fitted fragility functions for all collapse limit states. In this case, fragility functions related to r_u values are also calculated. Four values of the r_u are adopted to define the fragility functions (i.e. 95%, 75%, 50%, and 30%). However, for some of these values it was not possible to build fragility functions. For instance, the r_u in the alluvial sand never exceeds 50%, and in the sandy layer it never exceeds 30%, even for intense ground motions.

As shown in Table 7, CAV and CAV5 produce the lowest values of β, for both constitutive models. PGA and PGV values generally produce relatively low β values for all considered DMs, with PGA almost persistently producing lower β values than PGV. Overall, AI produces the highest β values. Figure 8 shows fragility functions for r_u as DMs. There are a number of occurrences when r_u is >0 does not increase as IMs increase. This might be related to the dilative behavior of some of the sandy layers, which result in the development of negative pore pressure. This implies that only where positive excess pore pressure is observed (i.e. contractive behavior), fragility functions show trends of increasing probabilities of damage with increasing values of the IM. The pit zone is the only case where there is a good fit of the fragility function, which is because the material located in this area has a contractive behavior. This is confirmed by the low β value for this fragility function.

Efficiency and predictability of ground motion intensity measures

Fragility function standard deviations (β values) cannot be used in isolation to define the optimal IM to adopt in forward analysis. As a result, in this section, we present the correlation between IMs and DMs for the Farneto del Principe and Angitola dams to evaluate

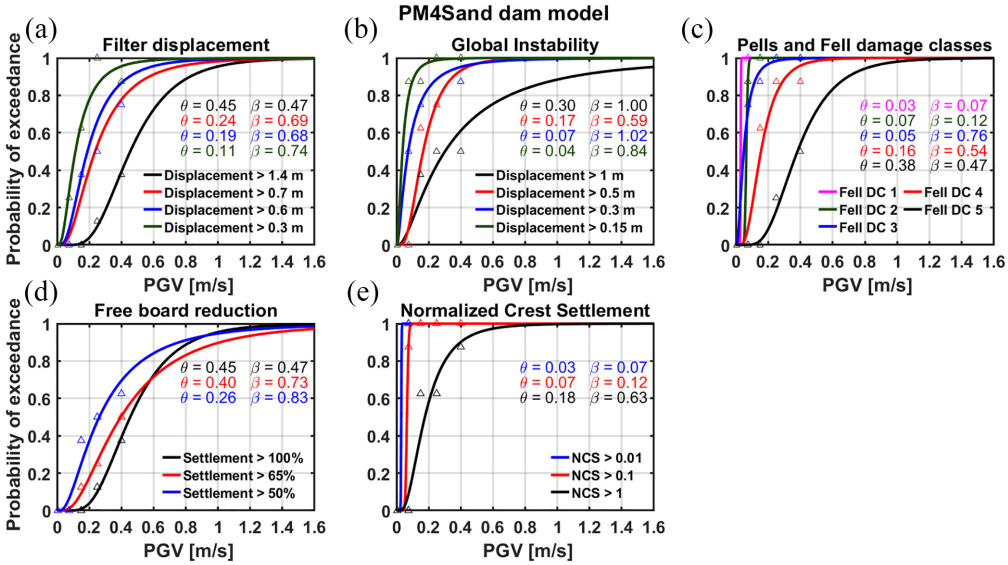

Figure 7. Fragility functions for the Angitola dam conditioned on PGV (PM4Sand dam model): (a) Filter displacement; (b) Global instability; (c) Fell damage classes; (d) Free board reduction; (e) Normalized Crest Settlement.

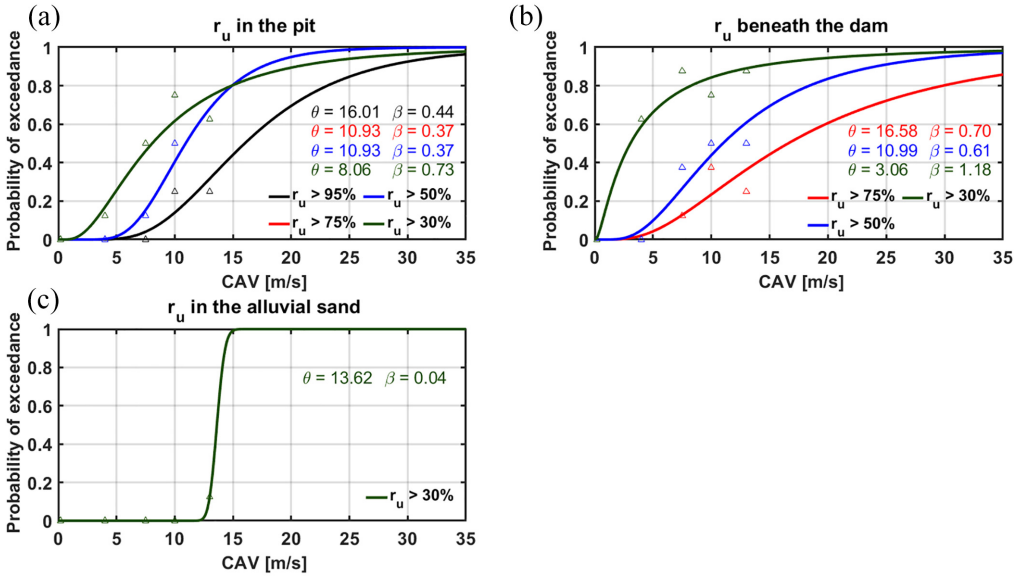

Figure 8. Fragility functions for the excess pore water pressure ratio r_u for the Angitola dam using CAV as Intensity Measure: (a) pit; (b) beneath the dam; (c) alluvial sand.

the efficiency of all analyzed IMs. An efficient IM will have a small value of the IM-DM correlation ($\sigma_{\ln\ DM|\ln\ IM}$). After the most efficient IMs are identified, an analysis on IM predictability is performed. Finally, both pieces of information, efficiency and predictability, are used together to determine the total standard deviation of each considered IM.

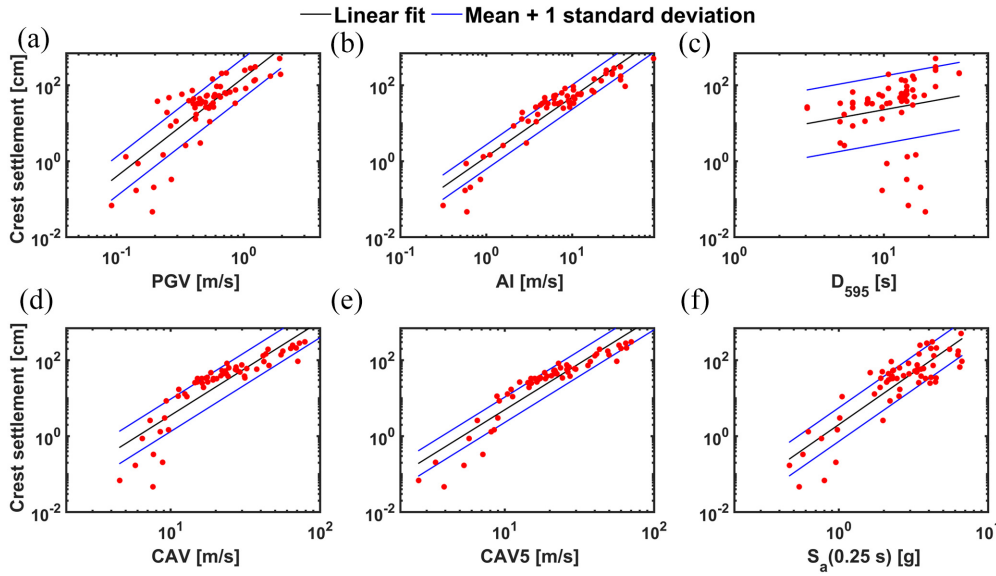

Figure 9. Ground motion IM efficiency for the crest settlement of the Farneto del Principe dam: (a) PGV; (b) AI; (c) D_{595}; (d) CAV; (e) CAV5; (f) Sa(0.25s).

This last parameter is believed to be the highest level synthetic parameter to guide the choice of an IM for forward deformation analysis (i.e. Armstrong et al., 2018a, 2021). Figure 9 shows the correlation between several IMs (PGV; AI; the significant duration: D_{595}, Trifunac and Brady, 1975; CAV, CAV5, and the spectral acceleration at 0.25s: S_a(0.25 s)) and the mean crest settlement for the Farneto del Principe dam. S_a(0.25 s) was chosen for this dam as it is the spectral acceleration corresponding to the estimated fundamental period of this dam (Zimmaro and Ausilio, 2020). In Figure 9, red points represent calculated damage, the linear regression line is reported in black, while blue lines are mean ± one standard deviation (i.e. 67% confidence interval bounds). Low values of the IMs (75 years of return period) are far from the mean. This evidence suggests a potentially biased correlation. Table 8 summarizes standard deviation values ($\sigma_{\ln DM|\ln IM}$) obtained for the Farneto del Principe dam, for the crest settlement. The significant duration D_{595} is the least efficient IM, as it results in high values of standard deviation. The most efficient IM is AI, followed by CAV. These results are consistent with findings by Armstrong et al. (2021) for dams in California. Armstrong et al. (2021) suggested that the evolutionary nature of AI and CAV (both being integral intensity measures) is the reason for their good efficiency.

Results obtained for the Angitola dam are illustrated in Figures 10 and 11, and Tables 9 and 10, for the MC and PM4Sand dam models, respectively. The IM-DM correlation is better than for the Farneto del Principe dam, which is reflected in the overall lower values of the $\sigma_{\ln DM|\ln IM}$ values. For the Angitola dam, we use the spectral acceleration at 0.2 s as this value is close to our estimate of its fundamental period.

For the PM4Sand dam model (Angitola dam), the most efficient IMs are AI, PGV, and CAV. Among them, CAV seems to be the most consistent, as it always stays in the range 0.50–0.53. The $\sigma_{\ln DM|\ln IM}$ values for the MC dam model, on the contrary, are slightly lower for almost all IMs, with CAV being particularly low. This is also consistent

Table 8. Efficiency, predictability, and total standard deviation for the Farneto del Principe dam, MC dam model, mean crest displacement, for PGV, AI, D_{595}, CAV, CAV5, and S_a(0.25 s) for some well-known ground motion models in the literature.

Farneto del Principe dam			
IM	Efficiency $\sigma_{\ln DM\|\ln IM}$ Crest displacement	Predictability $\sigma_{\ln IM\|\ln M,R,S}$	Total standard deviation $\sigma_{\ln DM\|\ln M,R,S}$
PGV [m/s]	1.194	0.652 (BSSA14)	2.074 (BSSA14)
		0.687 (AEA14)	2.149 (AEA14)
AI [m/s]	0.739	0.919 (CB)	1.626 (CB)
D_{595} [s]	2.044	0.419 (AS)	2.065 (AS)
CAV [m/s]	0.984	0.470 (CB)	1.523 (CB)
CAV5 [m/s]	0.768	0.708 (KM)	1.892 (KM)
S_a (0.25 s) [g]	1.021	0.621 (BSSA14)	1.986 (BSSA14)
		0.768 (AEA14)	2.340 (AEA14)
		0.780 (ZEA16)	2.370 (ZEA16)

IM: intensity measure; PGV: peak ground velocity; AI: Arias intensity; D_{595}: Significant duration; CAV: cumulative absolute velocity; CAV5: cumulative absolute velocity above 5 cm/s^2; S_a(0.25 s): spectral acceleration at 0.25s.

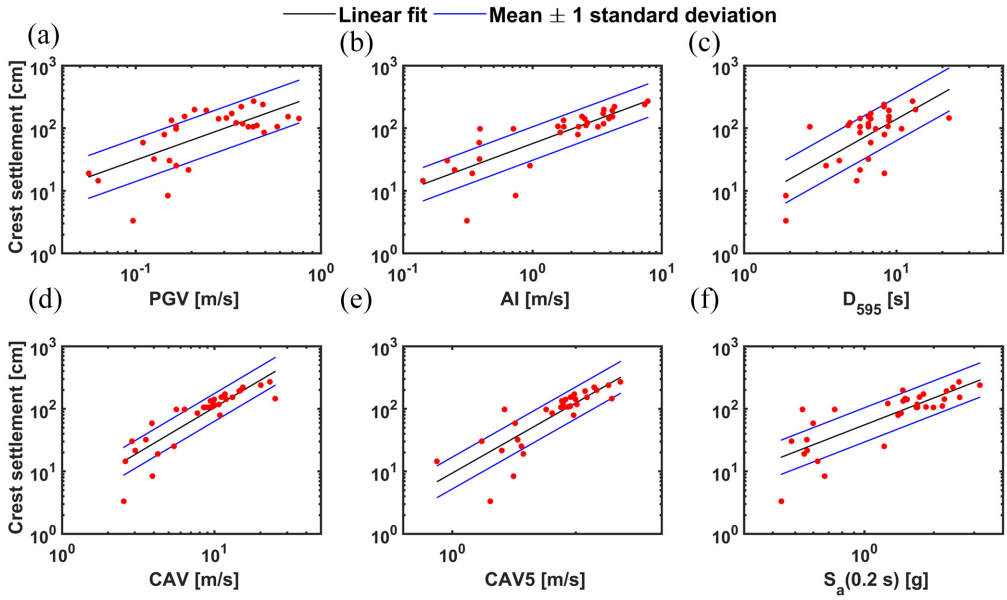

Figure 10. Ground motion intensity measure efficiency for the mean crest settlement for the Mohr-Coulomb dam model (Angitola dam): (a) PGV; (b) AI; (c) D_{595}; (d) CAV; (e) CAV5; (f) S_a(0.2s).

with findings by Armstrong et al. (2021), who found a higher level of variability in the case study where liquefaction phenomena may occur. This is a direct result of the complexity of damage mechanisms and damage patterns occurring when excess pore pressure–related phenomena occur. For the Angitola dam, only some zones experienced a r_u greater than 95%, but they were still sufficient to cause shear strength reduction effects and complex shear strain and deformation patterns, and thus a different response than what was observed using the MC model (which is not capable of accounting for excess pore pressure build-up and dissipation phenomena).

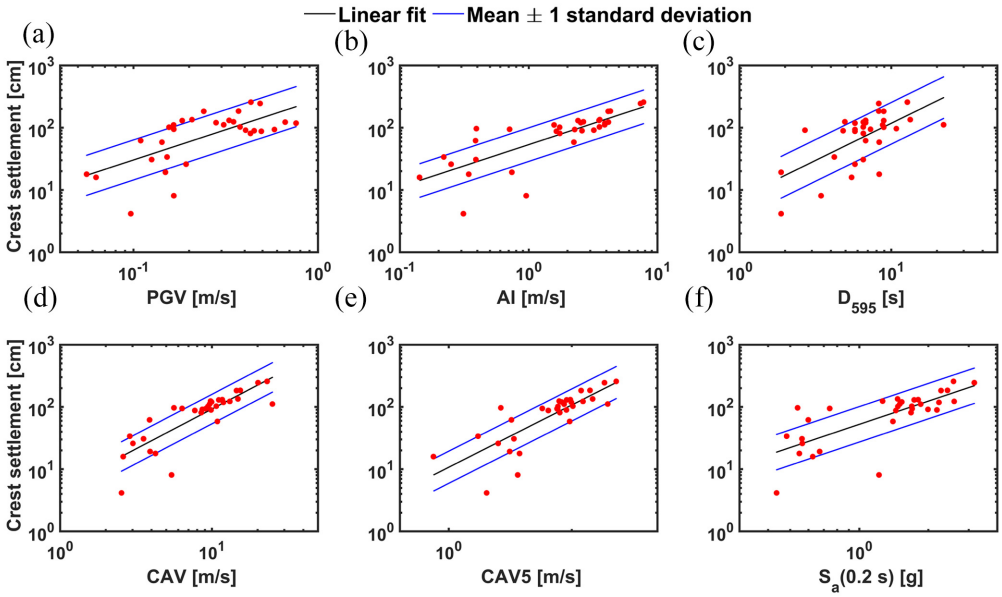

Figure 11. Ground motion intensity measure efficiency for the mean crest settlement for the PM4Sand dam model (Angitola dam): (a) PGV; (b) AI; (c) D_{595}; (d) CAV; (e) CAV5; (f) S_a(0.2s).

Table 9. Efficiency, predictability, and total standard deviation for the Angitola dam, MC dam model, mean crest displacement, PGV, AI, CAV, CAV5, and Sa(0.2 s) for some well-known ground motion models in the literature.

Angitola dam, Mohr-Coulomb dam model			
IM	Efficiency $\sigma_{\ln DM\|\ln IM}$ Crest displacement	Predictability $\sigma_{\ln IM\|\ln M,R,S}$	Total standard deviation $\sigma_{\ln DM\|\ln M,R,S}$
PGV [m/s]	0.788	0.652 (BSSA14)	1.047 (BSSA14)
		0.687 (AEA14)	1.072 (AEA14)
AI [m/s]	0.614	0.919 (CB)	0.936 (CB)
D_{595} [s]	0.792	0.419 (AS)	0.978 (AS)
CAV [m/s]	0.511	0.470 (CB)	0.850 (CB)
CAV5 [m/s]	0.586	0.708 (KM)	0.987 (KM)
S_a (0.2 s) [g]	0.631	0.621 (BSSA14)	1.089 (BSSA14)
		0.768 (AEA14)	1.265 (AEA14)
		0.780 (ZEA16)	1.281 (ZEA16)

IM: intensity measure; PGV: peak ground velocity; AI: Arias intensity; D_{595}: Significant duration; CAV: cumulative absolute velocity; CAV5: cumulative absolute velocity above 5 cm/s^2; S_a(0.2s): spectral acceleration at 0.2s.

As mentioned before, the efficiency of an IM cannot be the only parameter of reference when selecting an optimal IM for the estimation of earth dams deformation. This is especially so when recording stations are not available near the dam and IMs must be predicted using an empirical model. The analysis of IM sufficiency is outside the scope of this work, while IM predictability is incorporated in this study as suggested by Armstrong et al. (2021) by computing the total standard deviation as:

$$\sigma_{lnEDP\,|M,R,S} = \sqrt{\sigma^2_{lnEDP\,|lnIM} + b^2\sigma^2_{lnIM\,|M,R,S}} \tag{7}$$

Table 10. Efficiency, predictability, and total standard deviation for the Angitola dam, PM4Sand dam model, mean crest displacement, PGV, AI, CAV, CAV5, and Sa(0.2 s) for some well-known ground motion models in the literature.

Angitola dam, PM4Sand dam model			
IM	Efficiency $\sigma_{\ln DM\|\ln IM}$ Crest displacement	Predictability $\sigma_{\ln IM\|\ln M,R,S}$	Total standard deviation $\sigma_{\ln DM\|\ln M,R,S}$
PGV [m/s]	0.741	0.652 (BSSA14)	0.974 (BSSA14)
		0.687 (AEA14)	0.997 (AEA14)
AI [m/s]	0.621	0.919 (CB)	0.881 (CB)
D_{595} [s]	0.770	0.419 (AS)	0.919 (AS)
CAV [m/s]	0.545	0.470 (CB)	0.811 (CB)
CAV5 [m/s]	0.594	0.708 (KM)	0.924 (KM)
S_a (0.2 s) [g]	0.654	0.621 (BSSA14)	1.010 (BSSA14)
		0.768 (AEA14)	1.153 (AEA14)
		0.780 (ZEA16)	1.166 (ZEA16)

IM: intensity measure; PGV: peak ground velocity; AI: Arias intensity; D_{595}: Significant duration; CAV: cumulative absolute velocity; CAV5: cumulative absolute velocity above 5 cm/s^2; S_a(0.2s): spectral acceleration at 0.2s.

where $\sigma^2_{ln\,IM\ \ |M,R,S}$ is the standard deviation of a GMM, which represents its predictability, and b is the slope of the least-square linear regression in a log–log scale. GMM standard deviation values are from (1) Boore et al. (2014), BSSA14; (2) Akkar et al. (2014), AEA14; and (3) Zhao et al. (2016), ZEA16. GMM total standard deviations are estimated for the M and R that contribute the most to the seismic hazard for a return period of 1460 years.

For the standard deviation of AI and CAV, the Campbell and Bozorgnia, CB, (2019) model is used, while for CAV5 the Kramer and Mitchell relationship, KM (2006), is used. For the significant duration (D_{595}), the Afshari and Stewart GMM, AS (2016) was selected. For both analyzed dams, CAV is always the best IM (i.e. the IM with the lowest total standard deviation values). The second best IM is AI. CAV5 is the second best IM in terms of efficiency. However, it has poor predictability. Whenever monitoring stations are available, the IM with the best efficiency should be used. These results are generally consistent with those of Armstrong et al. (2018b, 2021). Similar results are obtained for the other DMs analyzed.

Tornado diagram analysis

The seismic assessment of critical infrastructure typically requires two steps: (1) the selection and scaling of hazard-consistent ground motions and (2) the evaluation of the seismic performance of the infrastructure being analyzed based on a numerical response history analysis. The former is usually accomplished with a site-specific PSHA, which in its general form comprises four components: (1) earthquake source characterization, (2) earthquake recurrence relationships, (3) ground motion models, and (4) computation of seismic hazard curves. PSHA results can then be used to produce response target spectra that are in turn adopted as the basis to select and scale hazard-consistent ground motions.

Each of the above steps carry uncertainties, as they can be undertaken at different levels of resolution. For instance, the source characterization can be performed with finite faults, background seismicity point sources, area sources, and/or combinations of these models. The choice of appropriate GMMs is also particularly challenging, since there may be a large number of GMMs that could be used at the site of interest. These uncertainties are

related to lack of knowledge about the phenomena being analyzed and are thus categorized as epistemic uncertainties. Such uncertainties are typically accounted for in a PSHA using the traditional logic tree approach. Robust PSHA models may produce a large number of branches (Porter et al., 2012). As a result, it is not possible to easily identify which branch(es) has the most influence on the seismic performance of the analyzed system. The concept of logic tree branches can also be adopted for numerical analyses to account for epistemic uncertainties (e.g. considering different choices for the strength of the materials or different constitutive models). Dam owners, managers, and/or stakeholders may need to define priorities on how and where to allocate funding to perform seismic re-evaluations of existing earth dams. This is particularly relevant as in Western countries most of these structures were built decades ago. As a result, in the remainder of this section, we explore the relative importance of PSHA- and numerical modeling–related choices and uncertainties in the seismic performance of earth dams. This analysis is performed departing from the Angitola dam case study. The tool used to perform this calculation is the tornado diagram (Porter, 2017; Porter et al., 2002). Tornado diagrams can be generated changing a single model parameter at a time, while keeping all of the others constant (typically assuming a high and low estimate of the quantity); this is repeated for all the variables of interest. The evaluation of the output variable of interest is performed and then the difference between the results obtained following this approach is calculated for each parameter (this is called swing).

Due to the computational cost limits, it is not always possible to perform NDAs for all of the possible parameters that come into play. In this article, three variables are selected and analyzed: (1) earthquake source characterization (or earthquake rupture forecast model, ERFM): using a site-specific model (i.e. with finite faults and area sources, Zimmaro and Stewart, 2017), and an off-the-shelf code-based model that only considers area sources (MPS Working Group, 2004); (2) the choice of the GMMs: one choice concerns more recent GMMs based on the methodology reported in Stewart et al. (2015) and the other choice is to use the same GMMs that are adopted in the Italian Building Code (Norme Tecniche per le Costruzioni (NTC), 2018), which date to 1996 (i.e. Ambraseys et al., 1996; Sabetta and Pugliese, 1996); and (3) the choice of the constitutive model (CM): a branch concerns the numerical model built using only the Mohr-Coulomb model coupled with a simplified hysteretic procedure (Itasca, 2019) and the other considering also the PM4Sand model to account for pore pressure–related effects. It should be noted that unlike variables such as material strength or loads, which are scalar quantities, the three variables adopted are nominal; thus, they can only have two values.

The tornado diagram analyses performed in this study refer to both: the Angitola dam (as analyzed in previous sections), and an idealized dam inspired by the Angitola dam, but with high potential of liquefaction in the dam body. Input parameters for this idealized, liquefiable dam are reported in Table 11. These analyses are performed using the MC and the PM4Sand models.

Figure 12 shows the eight branches adopted in the NDAs. For each branch, a PSHA is conducted, the UHS for a return period of 1460 years is defined (i.e. the return period associated with the collapse limit state for existing important dams in Italy), and seven ground motions are selected (in total there are 28 different ground motions). Then, the mean of a DM is taken (in this case, the crest settlement), and thus eight values are obtained. Finally, the influence of the following input choices: ERFM, GMM, and CM are estimated by calculating the tornado diagram swings. Since the analyzed variables are nominal, it is not straightforward to choose which values the other parameters should be

Table 11. PM4Sand parameters adopted for the shells of the idealized Angitola dam.

Property	Shells
D_R (%)	35
G_0	550
h_{p0}	4.8

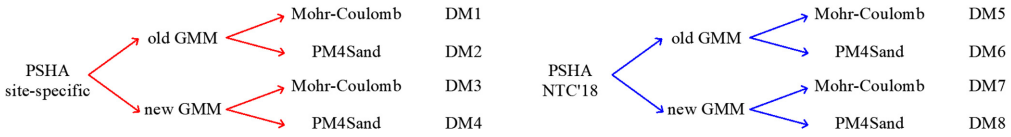

Figure 12. Branches used in the analyses. The baseline value is chosen as the median value of the eight possible values.

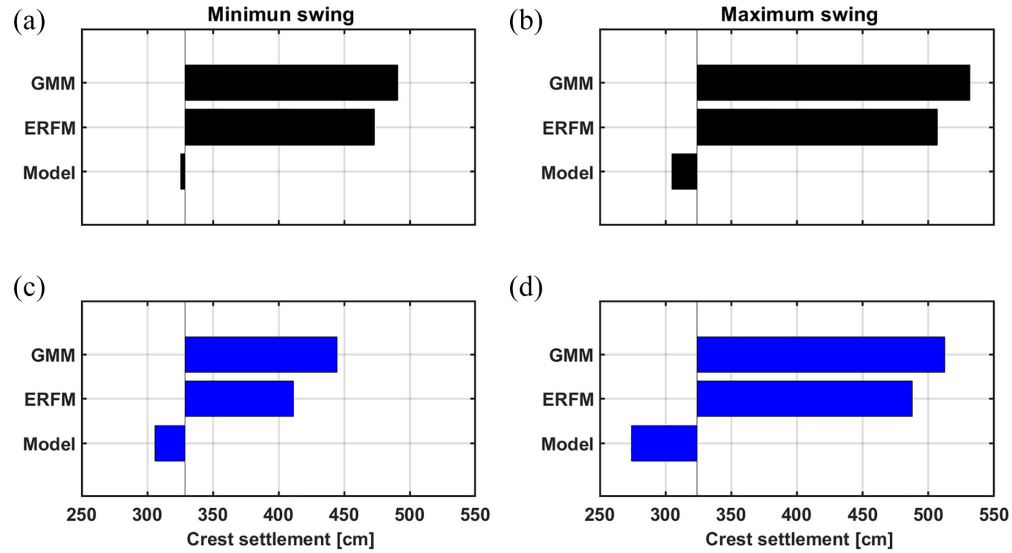

Figure 13. Tornado diagrams obtained from the analyses. Black swings refer to the Angitola dam with real properties (a) and (b). Blue swings refer to the idealized Angitola dam (c) and (d).

used (e.g. for scalar quantities, it would be a mean value). Thus, theoretically, four swings can be defined for each parameter. For instance, the CM swings are calculated as|DM1 – DM2,||DM3 – DM4,||DM5 – DM6,| and|DM7 – DM8.| For the sake of simplicity, in this study, the swings always refer to the maximum and minimum values of these four possibilities.

Figure 13 shows the tornado diagrams obtained from the analyses to a baseline value of crest settlement (i.e. the median of the eight outcomes). The black tornado refers to the Angitola dam with the real material properties, where little to any liquefaction deformations occur in the dam body; in this case, it can be seen that the swings related to the CM are limited. This is expected, since the PM4Sand model is built to analyze mainly

liquefaction-related issues. If no liquefaction occurs, the differences between advanced models and more simplified models are limited. As a result, when no substantial excess pore pressures are expected (i.e. if the dam is not strongly affected by liquefaction phenomena), the choice of appropriate ERFMs and GMMs are more important than the choice of the constitutive model. The choice of the GMM and ERFM, instead, results in a much more pronounced swing than that for the CM, with similar values. Thus, both models are extremely important in the overall performance of the dam in this case. For the fictitious dam, characterized by a more pronounced liquefaction-related hazard, the swing related to the CM is much greater (Figure 13c and d). This is because for dams more prone to liquefaction phenomena, the main failure mechanism observed is related to liquefaction deformations that occur at the base of the upstream shell.

The relative importance of these three variables can be appreciated by the differences between the three swings, which are represented graphically in Figure 13. For an earth dam susceptible to liquefaction in a high-seismicity area, none of the three parameters can be overlooked. If the dam is not expected to undergo significant liquefaction-related phenomena in the dam body, then the focus should be given to the choice of GMMs and ERFMs. Although the conclusions provided in this section should be strictly related to the dam being analyzed, we believe that the presented approach can be useful to guide prioritization of investments by dam owners/managers for similar dams. Furthermore, we presented a novel and repeatable approach to objectively derive quantitative insights that can be used to inform funding-allocation assessments for other dams in high seismic hazard regions.

Recommendations and conclusions

In this article, the seismic performance of two earth dams in Southern Italy is presented. These dams (the Farneto del Principe and the Angitola dams) are located in the same region and tectonic environment. However, the Angitola dam is founded on potentially liquefiable soils, whereas the Farneto del Principe dam only comprises non-liquefiable materials. The vulnerability of the two dams was assessed by means of analytical fragility functions. Fragility functions for different IMs and DMs were built and differences between constitutive models results were shown. In addition, the limit states that are more likely to be exceeded were estimated based on the comparison of the fragility functions at the same IM. Results from this study show that for both dams and almost all DMs, CAV- and CAV5-based fragility functions have the lowest standard deviation values. The availability of a large number of fragility functions for two typical earth dams in Italy will likely be used in the future to perform screening analyses and/or for the implementation of early warning systems on existing dams. Such simple preliminary studies on dams' vulnerability may be used to define priorities for future mitigation strategies of the entire national large dams inventory.

In the second part of the article, the correlation between IMs and DMs was addressed for both dams and all investigated IMs and DMs. CAV, CAV5, and PGV provided low values of efficiency. As a result, they were the most efficient IMs in predicting earth dam's damage. However, they do not have the same level of predictability. As a result, they can all be used in forward analyses only if recording stations are available at dams' sites. If input records for forward analyses need to be derived from global time series databases, efficiency and predictability need to be merged into one synthetic parameter to guide the selection of the best IM. This synthetic parameter was evaluated for all IMs and DMs.

CAV provided the lowest values of the total standard deviation for all IMs and DMs. Hence, it should be used for forward applications when recording stations are not available at the dam site.

Finally, we investigated the importance of three different modeling choices in the seismic performance of earth dams. Such analysis was performed by means of tornado diagrams and applied to the choice of appropriate constitutive models, ground motion models, and earthquake rupture forecast models. The idea behind this analysis is to provide dam owners and managers with a robust framework to perform prioritization and funding-allocation assessments. Our results show that the choices of appropriate GMMs and ERFM are always the driving factors for such analyses. We also show that for highly liquefiable dams (those were the dam body materials are susceptible to liquefaction), the use of a constitutive model capable of modeling pore pressure build-up and dissipation phenomena is recommended. On the contrary, if the deformation pattern of the dam is not expected to be substantially affected by liquefaction-related phenomena, simpler constitutive models can be used. In this case, the focus should be on the choice of GMMs and source characterization models.

Acknowledgments

The first author was in part co-financed by the University of Calabria through a Doctoral fellowship. This funding source is gratefully acknowledged. We thank Professor Giuseppe Lanzo at the University of Rome "La Sapienza" for sharing with us data and information pertaining to the geometry and geotechnical characterization of the Angitola dam. We thank Professor Steven L. Kramer at the University of Washington for the fruitful discussion on CAV vs CAV5 and on the CAV5 GMM he developed with Dr. Mitchell.

Declaration of conflicting interests

The author(s) declared no potential conflicts of interest with respect to the research, authorship, and/or publication of this article.

Funding

The author(s) received no financial support for the research, authorship, and/or publication of this article.

ORCID iD


Katerina Ziotopoulou https://orcid.org/0000-0001-5494-497X

Supplemental material

Supplemental material for this article is available online.

References

Afshari K and Stewart JP (2016) Physically parameterized prediction equations for significant duration in active crustal regions. *Earthquake Spectra* 32(4): 2057–2081.

Akkar S, Sandıkkaya MA and Bommer JJ (2014) Empirical ground-motion models for point- and extended-source crustal earthquake scenarios in Europe and the Middle East. *Bulletin of Earthquake Engineering* 12(1): 359–387.

Ambraseys NN, Simpson KA and Bommer JJ (1996) Prediction of horizontal response spectra in Europe. *Earthquake Engineering & Structural Dynamics* 25(4): 371–400.

Armstrong R, Kishida T and Park DS (2018a) Efficiency of ground motion intensity measures with earthquake-induced earth dam deformations. In: *Proceedings of the 2018 California strong motion instrumentation program seminar*, Sacramento, CA October 25, 2018.

Armstrong RJ (2018b) Relationship between earthquake ground motion intensity measures and embankment dam deformations. Final Report Submitted to California strong motion instrumentation program, California Geological Survey, Department of Conservation, June Sacramento, CA, USA.

Armstrong R, Kishida T and Park DS (2021) Efficiency of ground motion intensity measures with earthquake-induced earth dam deformations. *Earthquake Spectra* 37(1): 5–25.

Ausilio E, Dente G and Zimmaro P (2016) Geotechnical investigation and field performance of a zoned earth dam in Italy. In: *Proceedings of the 1st IMEKO TC4 international workshop on metrology for geotechnics*, Benevento, 16–18 March.

Baker JW (2011) Conditional mean spectrum: Tool for ground-motion selection. *Journal of Structural Engineering: ASCE* 137(3): 322–331.

Baker JW (2015) Efficient analytical fragility function fitting using dynamic structural analysis. *Earthquake Spectra* 31(1): 579–599.

Bernier C, Monteiro R and Paultre P (2016) Using the conditional spectrum method for improved fragility assessment of concrete gravity dams in Eastern Canada. *Earthquake Spectra* 32: 1449–1468.

Boore DM, Stewart JP, Seyhan E and Atkinson GM (2014) NGA-West2 equations for predicting PGA, PGV, and 5% damped PSA for shallow crustal earthquakes. *Earthquake Spectra* 30(3): 1057–1085.

Boulanger RW and Idriss IM (2014) *CPT and SPT based liquefaction triggering procedures*. Report no. UCD/CGM-14/01, April. Davis, CA: University of California, Davis April 2014.

Boulanger RW and Ziotopoulou K (2017) *PM4Sand (Version 3.1): A sand plasticity model for earthquake engineering applications*. Report no. UCD/CGM-17/01. Davis, CA: University of California, Davis. October 2017, revised January 2018.

Bray JD and Macedo J (2017) 6th Ishihara lecture: Simplified procedure for estimating liquefaction-induced building settlement. *Soil Dynamics and Earthquake Engineering* 102: 215–231.

Campbell KW and Bozorgnia Y (2019) Ground motion models for the horizontal components of Arias intensity (AI) and cumulative absolute velocity (CAV) using the NGA-West2 database. *Earthquake Spectra* 35(3): 1289–1310.

Di Sarno L and Elnashai AS (2021) Seismic fragility relationships for structures. In: Akkar S, Ilki A, Goksu C and Erdik M (eds) *Advances in Assessment and Modeling of Earthquake Loss*. Cham: Springer, pp. 189–222.

Dorsey C (2011) *Memorandum of Design Review Leroy Anderson Dam No. 72-9 Santa Clara County*. Sacramento, CA: Division of Safety of Dams—California.

Figura F (2020) *Comportamento dinamico della diga in terra nel comune di Briaglia: definizione delle curve di fragilità*. Master's thesis. Turin: Politecnico di Torino.

Hurtado-López G and Mayoral-Villa J (2020) Fragility curves for hardfill dams under seismic loading Curvas de fragilidad para presas de *hardfill* bajo carga sísmica. *Tecnología y ciencias del agua* 11(1): 132–168.

Itasca (2019) *Fast Lagrangian Analysis of Continua (FLAC)—Version 8.1, User's Guide*. Minneapolis, MN: Itasca Consulting Group.

Jin C and Chi S (2019) Seismic fragility analysis of high earth-rockfill dams considering the number of ground motion records. *Mathematical Problems in Engineering* 2019: 6958643.

Joint Research Centre, Institute for the Protection and Security of the Citizen, Taucer F, Hancilar U, Iervolino I, et al., Guidelines for deriving seismic fragility functions of elements at risk: buildings, lifelines, transportation networks and critical facilities, Taucer, F. (editor), Hancilar, U. (editor), Kaynia, A. (editor), Publications Office, 2013. Issued on 31 March 2013.

Karimi Z and Dashti S (2017) Ground motion intensity measures to evaluate II: The performance of shallow-founded structures on liquefiable ground. *Earthquake Spectra* 33: 277–298.

Kramer SL and Mitchell RA (2006) An efficient and sufficient scalar intensity measure for soil liquefaction. *Earthquake Spectra* 22(2): 1–26.

Kuhl J (2011) *Memorandum of Design Review James J. Lenihan Dam No. 72-8 Santa Clara County*. Sacramento, CA: Division of Safety of Dams—California, pp. 1–27.

Kwak DY, Stewart JP, Brandenberg SJ and Mikami A (2016) Characterization of seismic levee fragility using field performance data. *Earthquake Spectra* 32(1): 193–215.

Lin T, Haselton CB and Baker JW (2013) Conditional spectrum-based ground motion selection. Part I: Hazard consistency for risk-based assessments. *Earthquake Engineering & Structural Dynamics* 42(12): 1847–1865.

Luco N and Cornell CA (2001) Structure-specific scalar intensity measures for near-source and ordinary earthquake ground motions. *Earthquake Spectra* 23: 357–392.

Lysmer J and Kuhlemeyer RL (1973) Finite dynamic model for infinite media. *Journal of the Engineering Mechanics Division: ASCE* 95(4): 859–877.

MPS Working Group (2004) Redazione della mappa di pericolosità sismica prevista dall'Ordinanza PCM del 20 marzo 2003, n. 3274, All.1. Rapporto conclusivo per il Dipartimento della Protezione Civile, Istituto Nazionale di Geofisica e Vulcanologia (INGV), Roma, April.

Nguyen D-D, Lee T-H and Phan V-T (2021) Optimal earthquake intensity measures for probabilistic seismic demand models of base-isolated nuclear power plant structures. *Energies* 14: 5163.

Norme Tecniche per le Costruzioni (NTC) (2018) *Ministero delle Infrastrutture e dei Trasporti*. Aggiornamento delle Norme Tecniche per le Costruzioni, D.M.17-1-2018. Gazzetta Ufficiale del la Repubblica Italiana, no. 42. Available at: https://www.gazzettaufficiale.it/eli/id/2018/2/20/18A00716/sg (accessed, april 2023).

Pagano L and Sica S (2012) Earthquake early warning for earth dams: Concepts and objectives. *Natural Hazards* 66: 303–318.

Pells S and Fell R (2003) Damage and cracking of embankment dams by earthquake and the implications for internal erosion and piping. In: *Proceedings of the 21st international congress on large dams (ICOLD)*, Montreal, QC, Canada June 2003.

Penman ADM (1986) On the embankment dam. *Geotechnique* 36: 301–348.

Porter KA, Beck JL and Shaikhutdinov RV (2002). Sensitivity of building loss estimates to major uncertain variables. *Earthquake Spectra*, 18 (4), 719–743.

Porter K (2017) *A Beginner's Guide to Fragility, Vulnerability, and Risk*. Boulder, CO: University of Colorado Boulder, 103 pp.

Porter KA, Field EH and Milner K (2012) Trimming the UCERF2 hazard logic tree. *Seismological Research Letters* 83(5): 815–828.

Rathje EM and He J (2022) A seismic fragility framework for earth dams. In: *Proceedings of the lifelines 2022: 1971 San Fernando earthquake and lifeline infrastructure—ASCE*, University of California, Los Angeles, Los Angeles, CA, 31 January–11 February.

Regina G (2021) *Probabilistic assessment of the seismic performance of two earth dams in Southern Italy using simplified and advanced constitutive models*. PhD Dissertation, University of Calabria, Rende.

Regina G, Ausilio E, Dente G and Zimmaro P (2021) A critical overview of geophysical investigation and laboratory test results used in the seismic re-evaluation of the Farneto del Principe dam in Italy. In: *Proceedings of the 6th international conference on geotechnical and geophysical site characterization*, Budapest, 26–29 September.

Sabetta F and Pugliese A (1996) Estimation of response spectra and simulation of nonstationary earthquake ground motions. *Bulletin of the Seismological Society of America* 86: 337–352.

Seed HB (1979) Soil liquefaction and cyclic mobility evaluation for level ground during earthquakes. *Journal of the Geotechnical Engineering Division: ASCE* 105(2): 201–255.

Stewart JP, Douglas J, Javanbarg M, Bozorgnia Y, Abrahamson NA, Boore DM, Campbell KW, Delavaud E, Erdik M and Stafford PJ (2015) Selection of ground motion prediction equations for the Global Earthquake Model. *Earthquake Spectra* 31(1): 19–45.

Swaisgood JR (2003) Embankment dam deformations caused by earthquakes. In: *Proceedings of the 2003 Pacific conference on earthquake engineering*, Christchurch, New Zealand, 13–15 February.

Swaisgood JR (2014) Behavior of embankment dams during earthquake. *Journal of Dam Safety: ASDSO* 12(2): 35–44.

Trifunac MD and Brady AG (1975) A study on the duration of strong earthquake ground motion. *Bulletin of the Seismological Society of America* 65: 581–626.

Tsai Y-T (2018) *Characterizing seismic performance of levees on peaty organic soils from case histories and simulations*. PhD Thesis, University of California, Los Angeles, Los Angeles, CA.

Vecchietti A, Cecconi M, Russo G and Pane V (2019) Seismic vulnerability of a rockfill dam through different displacement-based approaches. *Journal of Earthquake Engineering* 26: 1–27.

Wong IG and Thomas P (2017) Comparing seismic hazard estimates for dams in the US and their implications to risk. In: *Proceedings of the 2017 association of state dam safety officials conference*, San Antonio, TX, 10–14 September.

Yang Y (2021) *Calibrated fragility functions for seismic loading of Sacramento—San Joaquin River Delta levees*. PhD Dissertation, University of California, Los Angeles, Los Angeles, CA, 259 pp.

Zhao JX, Zhou SL, Zhou J, Zhao C, Zhang H, Zhang YB, Gao PJ, Lan X, Rhoades DA, Fukushima Y, Somerville PG and Irikura K (2016) Ground-motion prediction equations for shallow crustal and upper-mantle earthquakes in Japan using site class and simple geometric attenuation functions. *Bulletin of the Seismological Society of America* 106: 1552–1569.

Zimmaro P and Ausilio E (2020). Numerical Evaluation of Natural Periods and Mode Shapes of Earth Dams for Probabilistic Seismic Hazard Analysis Applications. *Geosciences*, 10(12), 499.

Zimmaro P and Stewart JP (2017) Site-specific seismic hazard analysis for Calabrian dam site using regionally customized seismic source and ground motion models. *Soil Dynamics and Earthquake Engineering* 94: 179–192.